Journal of Advanced Ceramics
2016, **5**(3): 219–224
DOI: 10.1007/s40145-016-0193-1

ISSN 2226-4108
CN 10-1154/TQ

Research Article

Enhanced energy storage properties of $Bi_{0.5}Li_{0.5}TiO_3$ modified $Sr_{0.1}Bi_{0.45}Na_{0.45}TiO_3$ based ceramics

Qin FENG[a,b], Xiao LIU[c], Changlai YUAN[b,*], Xinyu LIU[a,b], Changrong ZHOU[b], Guohua CHEN[b]

[a]*College of Material Science and Engineering, Central South University, Changsha 410083, China*
[b]*College of Material Science and Engineering, Guilin University of Electronic Technology, Guilin 541004, China*
[c]*College of Powder Metallurgy Research Institute, Central South University, Changsha 410083, China*

Received: April 03, 2016; Revised: May 24, 2016; Accepted: May 30, 2016

Abstract: Lead-free $(1-x)Sr_{0.1}Bi_{0.45}Na_{0.45}TiO_3$–$xBi_{0.5}Li_{0.5}TiO_3$ ($x = 0$–0.4) ceramics were successfully prepared by a solid-state reaction technique. The effects of amount of $Bi_{0.5}Li_{0.5}TiO_3$ on structure and electrical properties were examined. The X-ray diffraction (XRD) analysis revealed that all the investigated specimens have a perovskite structure. An obvious change in microstructure with the increase of $Bi_{0.5}Li_{0.5}TiO_3$ concentration was observed. This study demonstrated that relaxor could be stabilized in $Sr_{0.1}Bi_{0.45}Na_{0.45}TiO_3$ based ceramics by lowering the tolerance factor and electronegativity difference. Besides, a dielectric anomaly related to thermal evolution of crystallographic symmetry was emerged at the depolarization temperature. Upon incorporation of 26 mol% $Bi_{0.5}Li_{0.5}TiO_3$, the specimens were able to withstand an electric field intensity of 106.9 kV/cm with an energy density of 0.88 J/cm^3 and an energy efficiency of 65%.

Keywords: energy storage; ferroelectricity; $Bi_{0.5}Li_{0.5}TiO_3$

1 Introduction

In response to the current environmental regulations against the use of lead in daily electronic devices, ceramics with a perovskite structure have been of great interest to the community. The presence of interstitial sites and relatively large spatial tolerance for substitution atoms are beneficial for chemical modifications and enabling perovskite structure to tailor electrical properties [1]. Among various perovskite-type materials, $Bi_{0.5}Na_{0.5}TiO_3$ (BNT) is considered as one of the most competitive alternatives for lead based ceramics. BNT is a typical perovskite structure ferroelectric material with 1:1 ratio of Na^+ and Bi^{3+} at A-site, which causes high polarization due to the existence of stereo-chemically active long pair electrons [2]. Therefore, it is also a candidate for energy storage dielectric. However, pure BNT ceramic is a typical ferroelectric (FE) substance suffering for large polarization loss which limits its application in practice.

Recently, binary and ternary system relaxor ceramics have been investigated for their high energy storage application, e.g., BNT–$BaTiO_3$ [3], BNT–$BaTiO_3$–$K_{0.5}Na_{0.5}NbO_3$ [4–6], BNT–$BaTiO_3$–$NaNO_3$ [7], BNT–$CaTiO_3$ [8], BNT–$SrTiO_3$–$BaTiO_3$ [9], BNT–$K_{0.5}Bi_{0.5}TiO_3$–$BaTiO_3$ [10], etc. The decreased remnant polarization (P_r) value, which is favored to receive larger recoverable energy density compared with pure BNT, is found in these systems. As reported, the discharged energy density (J_d) of BNT based ceramics

* Corresponding author.
E-mail: yclguet@yahoo.com, yclai-2002@163.com

is ranged from 0.6 to 0.9 J/cm^3 if no glass phase is added. Among these systems, $Sr_{0.1}Bi_{0.45}Na_{0.45}TiO_3$ (SBNT) has attracted much attention due to its strong dispersion of the permittivity with a relaxor-like behavior [11–13]. Besides, the alkali metal ion of Li^+, which is in the same group as Na^+ and K^+ in periodic table of elements, has the similar properties. Based on the above, in this paper, $(1–x)Sr_{0.1}Bi_{0.45}Na_{0.45}TiO_3–xBi_{0.5}Li_{0.5}TiO_3$ (SBNT–*x*BLT) are selected as lead-free energy storage materials and investigated for the dependence of structure and electrical properties on composition (x). In addition, the energy storage properties of SBNT–*x*BLT ($0 \leqslant x \leqslant$ 40 mol%) ceramics are demonstrated in detail.

2 Experiment

SBNT–*x*BLT ($x = 0.00$, 0.20, 0.24, 0.26, 0.30, and 0.40, abbreviated as N1, N2, N3, N4, N5, and N6, respectively) ceramics were prepared by a mixed oxide route from appropriate quantities of high purity ($\geqslant$ 99.9%) Li_2CO_3, $SrCO_3$, Bi_2O_3, Na_2CO_3, and TiO_2. The starting materials were mixed and grounded in alcohol for 9 h with ZrO_2 balls. Then, the mixture was dried and calcined at 870 ℃ for 2 h. The resultant powders were mixed with 5 wt% of polyvinyl alcohol as binder and pressed into pellets of 10 mm in diameter and 1 mm in thickness by uniaxial pressing. Then, dense pellets were obtained by sintering in air at 1020 ℃ for 4 h. The crystal phases of the sintered ceramics were analyzed using an X-ray diffractometer (Model D8-Advance, Bruker, Germany). The microstructural observation of the crystallized samples was carried out using a field emission scanning electron microscope (FE-SEM, Model S-4800, Hitachi, Japan). For electrical measurements, each of pellet faces was coated with Ag electrode. The polarization–electric field hysteresis loops were measured using a ferroelectric tester (Precision Premier II, USA) with a frequency of 1 Hz, and the energy density was estimated from the *P–E* curves by integrating the area enclosed within the polarization axis and the discharged curve. The temperature-dependent dielectric properties were measured at 1 kHz by an Agilent HP4294A analyzer, with heating and cooling controlled conditions in an oven. The breakdown strength (BDS) was determined by a DC bias source (Model MARX, Tianjin Dongwen Company, China). For each composition, at least 6 samples were measured to obtain the average BDS.

3 Results and discussion

The structures of all the samples were characterized by X-ray diffraction (XRD), as presented in Fig. 1, and the results are identified by a pseudocubic symmetry (PDF Card No. 81-2200) for $x \leqslant 0.2$ within the sensitivity of XRD [14]. Meanwhile, a secondary phase indexed as Li_2TiO_3 appears with $x > 0.2$, although its content is found only in trace amount. The FE-SEM micrographs of the samples are shown in Fig. 2. The average grain size for the pristine ceramic is much less than the others. Besides, with the increase of BLT concentration, the grain size distribution gradually becomes uniform. The result suggests that a certain amount of additive of BLT will result in increasing grain size and affect their electrical properties accordingly.

Tolerance factor (t) and electronegativity difference (X) can be used to assess the rational design of stability in perovskite. Lead-containing ceramics possess double *P–E* loops with both low t and X. Compared to complex lead perovskite compounds, lead-free perovskite phase is more stabilized via solid solutions when t or X is increased. On the contrary, a relaxor phase, which exhibits a pseudocubic symmetry in average with the presence of non-polar below the detection limit of XRD technique, can be stabilized by decreasing the value of t [15], e.g., Nd-doped $BiFeO_3$ displays double *P–E* loops that is attributed to a decrease in t [16,17]. The Goldschmidt tolerance factor t and electronegativity difference X, are given by Eq. (1) and Eq. (2) respectively:

$$t = (R_A + R_O) / [2^{1/2}(R_B + R_O)] \quad (1)$$

$$X = (X_{AO} + X_{BO}) / 2 \quad (2)$$

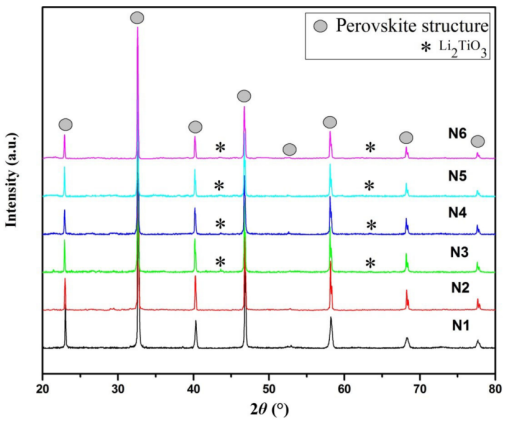

Fig. 1 XRD patterns of the SBNT–*x*BLT ($0 \leqslant x \leqslant 0.4$) ceramics.

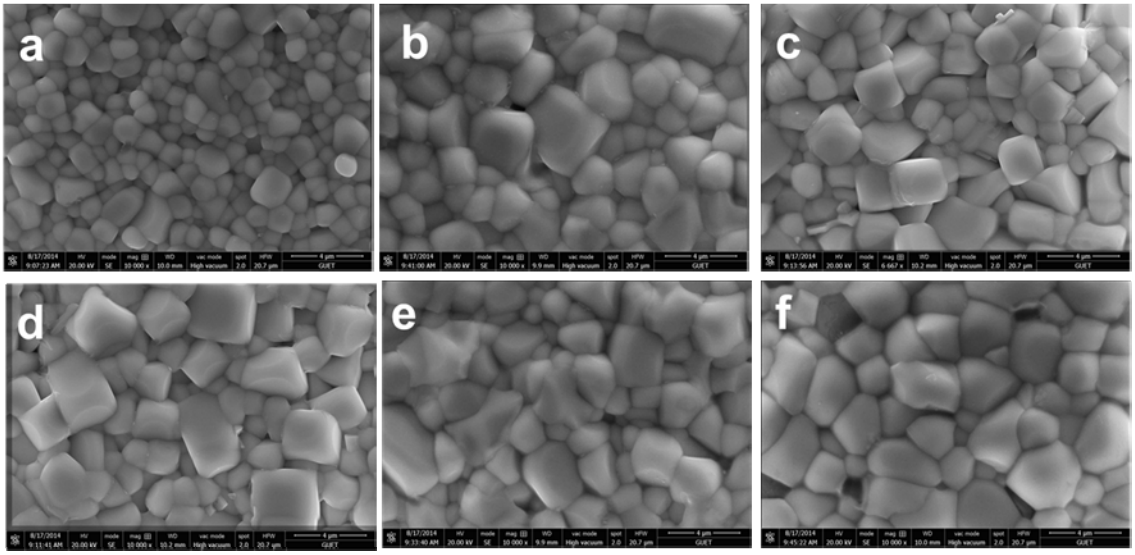

Fig. 2 FE-SEM images of the samples sintered at 1020 ℃: (a) N1, (b) N2, (c) N3, (d) N4, (e) N5, and (f) N6.

where R_A, R_B, and R_O are ionic radii for the A- and B-site cations and the oxygen anion, respectively. X_{AO} and X_{BO} are the electronegativity difference of A cation and B cation with oxygen anion, respectively. Figure 3 shows a linear relationship between t and X for SBNT–xBLT compositions. With the increase of the BLT concentration, both t and X decrease gradually and SBNT–xBNT ceramics, therefore, are expected to approach a square P–E loop. Meanwhile, the relaxor phase will become more and more stable, which is manifested in the follow-up experiments.

A set of temperature-dependent dielectric measurements on SBNT–xBLT ceramics, given in Fig. 4, confirms that the changes of dielectric constant induced by compositional modifications are apparent. The dielectric properties of pure SBNT ceramic are featured with a distinct dielectric anomaly at T_m (~250 ℃), as marked in the figure. Compared to the pristine ceramic, the BLT-added ceramics exhibit another dielectric anomaly with $0.2 \leqslant x \leqslant 0.3$, locating at depolarization temperature T_f (~90 ℃). The corresponding dielectric loss in the inset (a) of Fig. 4 also possesses a peak, which can be ascribed to that the polar nanoregions (PNRs) transform into microsized domains at T_f [18]. And PNRs are also the origin of relaxation behavior for SBNT–0.2BLT ceramic around T_f, as seen in the inset (b) of Fig. 4. Simultaneously, the dielectric constant decreases and the curves become more flat with increasing BLT concentration. Previously, this anomaly was believed to be attributed to thermal evolution of ferroelectric polar and weakly polar [19] or non-polar symmetry [7].

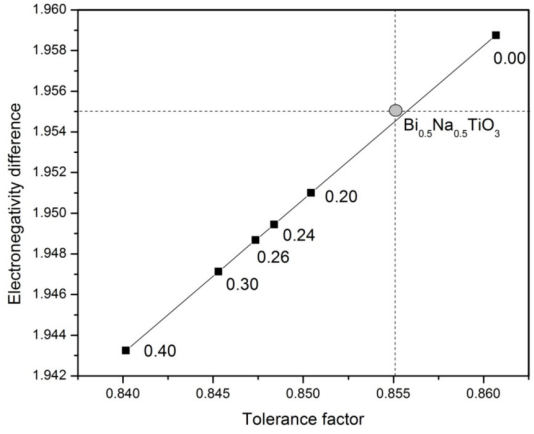

Fig. 3 Tolerance factor versus averaged electronegativity difference for SBNT–xBLT ($0 \leqslant x \leqslant 0.4$) ceramics.

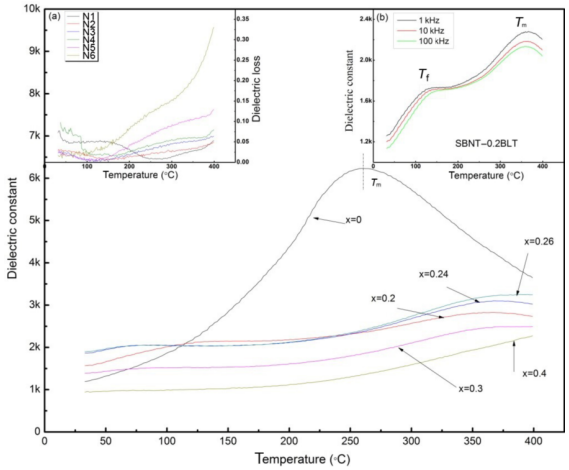

Fig. 4 Temperature dependence of dielectric constant for SBNT–xBLT ($0 \leqslant x \leqslant 0.4$) ceramics. Inset (a): temperature dependence of dielectric loss; inset (b): frequency and temperature dependence of dielectric constant for SBNT–0.2BLT ceramic.

Figure 5 shows the Weibull distribution of the breakdown strength (BDS) for SBNT–*x*BLT ceramics with different BLT concentrations. The Weibull linear equation, as a widely acceptable model, is always employed to calculate the reasonable values of BDS. The plot can be expressed by the following relationships:

$$X_i = \ln E_i \tag{3}$$

$$Y_i = \ln\left(-\ln\left(1-\frac{i}{n+1}\right)\right) \tag{4}$$

where E_i is the specific breakdown value of each specimen in the experiments, n is the sum of specimens, i is the serial number of the specimens, and the specimens are arranged in ascending order of BDS values so that $E_1 \leqslant E_2 \leqslant \cdots \leqslant E_i \leqslant \cdots \leqslant E_n$. Obviously, all the slopes (m) of the Weibull curves are linear, and $m > 1$; it indicates that the BDS can be analyzed by the Weibull model. The values of BDS as a function of BLT addition are shown in the inset of Fig. 5. As the BLT concentration increases up to 26 mol%, the breakdown strength of the ceramic samples increases from 48.1 (x = 0) to 106.9 kV/cm (x = 0.26). With the further increase of BLT content, the values of BDS decrease gradually. It was reported that the breakdown strength is closely related to activation energy (E_a) and grain size [20–22]. According to the experiment results, E_a is the most likely driving force for breakdown strength variation, and the change of grain size is unnoticeable when the BLT concentration exceeds 20 mol% (as seen in Fig. 2).

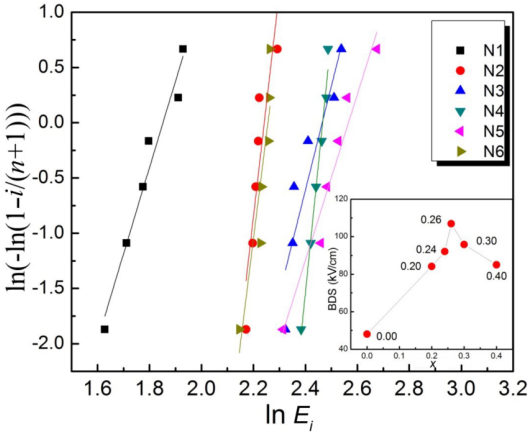

Fig. 5 Weibull plots of dielectric breakdown strength.

The energy storage behavior of the SBNT–*x*BLT ceramics with the same electric field is investigated in terms of the polarization–electric field (*P*–*E*) hysteresis loops. Figure 6 displays hysteresis loops of SBNT–*x*BLT ceramics measured with a frequency of 1 Hz at room temperature. A massive alignment of randomly-oriented ferroelectric domains occurs in BNT ceramics along the field direction by switching its polarity towards one of the energetically equivalent directions [1]. As mentioned before, a reduction in tolerance factor and electronegativity difference can contribute to the lessening of the relative stability of the FE structure. As a result, a greater fraction of reoriented ferroelectric domains switch back with the removal of the applied electric field, leaving the material reach a reduced remanent state. And this corresponds to the

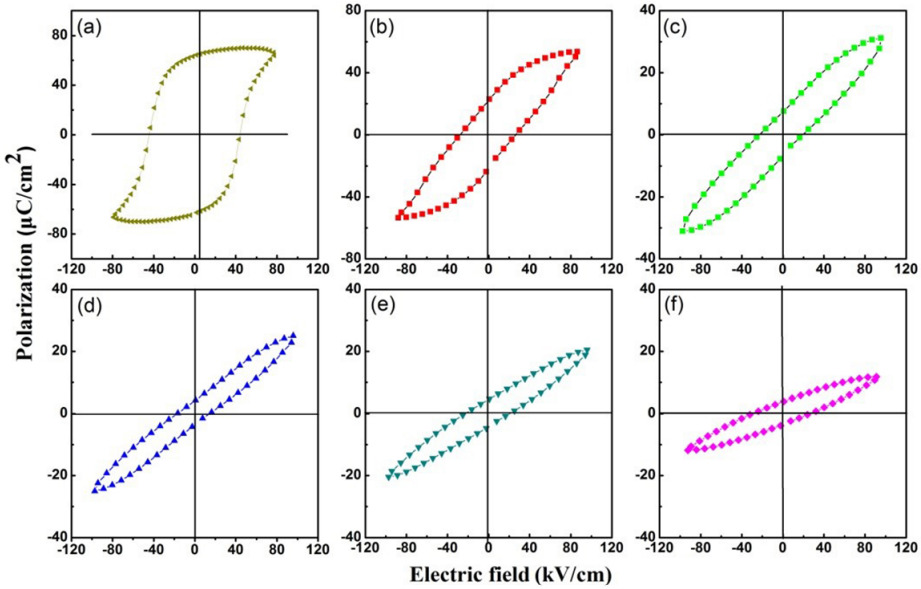

Fig. 6 *P*–*E* hysteresis loops of the SBNT–*x*BLT ($0 \leqslant x \leqslant 0.4$) ceramics.

evolution of *P*–*E* loops in Fig. 6. However, the so called "non-polar phase" is too stable to induce a ferroelectric state out of a relaxor state under the same external applied electric field in N5 and N6, as shown in Figs. 6(e) and 6(f), respectively.

The discharged energy density is obtained by integrating the area between the polarization axis and the discharge curve in the first quartile of *P*–*E* hysteresis loops [23]. According to the definition of discharged energy density, saturated polarization and remnant polarization have a direct impact on it. It is observed that with the increase of the BLT concentration, the saturated polarization (P_s) decreases gradually. Meanwhile, the remnant polarization first decreases sharply and then almost remains constant. Figure 7 shows the discharged energy density of the samples sintered at 1020 ℃ as a function of electric field at room temperature. The nonlinear behavior, with increasing electric field, is observed for all the cases. Obviously, higher applied electric field is more conducive to energy storage capability. Pure SBNT ceramic has the lowest discharged density, owing to the rather slow kinetics of reoriented domains back switching. The increasing concentration of BLT leads to a sharp drop in remnant polarization, which improves energy storage properties gradually. Consequently, a maximum energy storage density of 0.88 J/cm^3 under an applied field 95 kV/cm is achieved when the increasing content of BLT up to 26 mol%. Thereafter, the energy storage properties deteriorate as BLT further increases. The energy efficiency (η) is defined as the ratio of the energy density discharged to the energy density charged (J_c). As presented in Fig. 8, the energy efficiencies of BLT-added specimens are obviously enhanced, showing the values in the range of 60% –75% at 60–90 kV/cm. The polarization retention behavior is believed to be the scenario to explicate the difference between J_d and J_c in a charge–discharge cycle. For the BLT-added specimens, reoriented ferroelectric domains switch back rapidly depending on their energetic stability with the removal of the applied electric field, resulting in a depressed poling process in the grains. Consequently, the BLT-added specimens achieve higher energy efficiencies as compared to the pristine specimen. However, the increase of the external applied electric field will expand the gap between J_d and J_c, and the corresponding energy efficiencies of SBNT–0.26BLT specimen initially at around 88% then gradually decrease to ~65%.

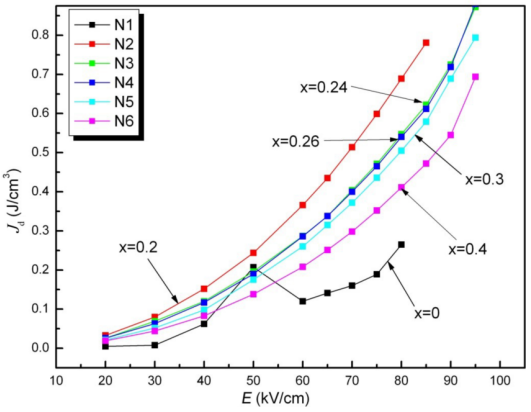

Fig. 7 Discharged energy density of all the samples as a function of electric field at room temperature.

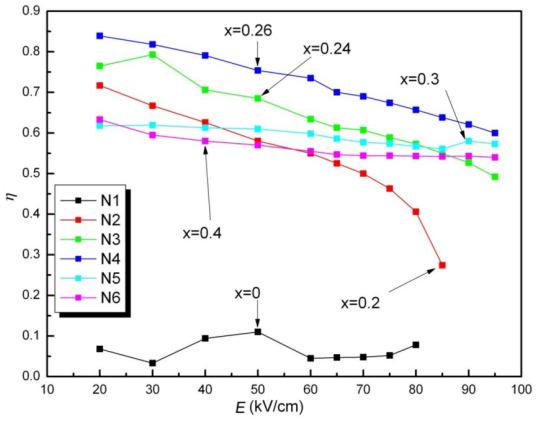

Fig. 8 Energy efficiency of all the samples as a function of electric field at room temperature.

4 Conclusions

$(1–x)Sr_{0.1}(Bi_{0.5}Na_{0.5})_{0.9}TiO_3–xBi_{0.5}Li_{0.5}TiO_3$ ceramics with different content x were fabricated by solid-state reaction method. The effects of x values on the microstructure, ferroelectric properties (including the energy storage density), and dielectric properties were studied. XRD results of all the samples exhibited a typical perovskite structure. In the system, the BLT showed a strong influence on the microstructure, dielectric constant, BDS, and energy density. Besides, a maximum recoverable energy storage density of 0.88 J/cm³ with a high BDS of 106.9 kV/cm was achieved. These results showed that SBNT–BLT ceramics are a promising candidate dielectric material for high voltage, high energy density capacitors.

Acknowledgements

Financial supports of the National Natural Science

Foundation of China (Grant Nos. 11464006, 61561011, and 51462005) and the Natural Science Foundation of Guangxi (Grant No. 2014GXNSFBA118254) are gratefully acknowledged by the authors.

References

[1] Jo W, Dittmer R, Acosta M, *et al*. Giant electric-field-induced strains in lead-free ceramics for actuator applications—status and perspective. *J Electroceram* 2012, **29**: 71–93.

[2] Barick BK, Choudhary RNP, Pradhan DK. Dielectric and impedance spectroscopy of zirconium modified $(Na_{0.5}Bi_{0.5})TiO_3$ ceramics. *Ceram Int* 2013, **39**: 5695–5704.

[3] Guo Y, Akai D, Sawada K, *et al*. Structure and electrical properties of trilayered $BaTiO_3/(Na_{0.5}Bi_{0.5})TiO_3$–$BaTiO_3/BaTiO_3$ thin films deposited on Si substrate. *Solid State Commun* 2009, **149**: 14–17.

[4] Viola G, Ning H, Reece MJ, *et al*. Reversibility in electric field-induced transitions and energy storage properties of bismuth-based perovskite ceramics. *J Phys D: Appl Phys* 2012, **45**: 355302.

[5] Wang B, Luo L, Jiang X, *et al*. Energy-storage properties of $(1-x)Bi_{0.47}Na_{0.47}Ba_{0.06}TiO_3$–$xKNbO_3$ lead-free ceramics. *J Alloys Compd* 2014, **585**: 14–18.

[6] Ding J, Liu Y, Lu Y, *et al*. Enhanced energy-storage properties of $0.89Bi_{0.5}Na_{0.5}TiO_3$–$0.06BaTiO_3$–$0.05K_{0.5}Na_{0.5}NbO_3$ lead-free anti-ferroelectric ceramics by two-step sintering method. *Mater Lett* 2014, **114**: 107–110.

[7] Xu Q, Li T, Hao H, *et al*. Enhanced energy storage properties of $NaNbO_3$ modified $Bi_{0.5}Na_{0.5}TiO_3$ based ceramics. *J Eur Ceram Soc* 2015, **35**: 545–553.

[8] Yuan Y, Zhao CJ, Zhou XH, *et al*. High-temperature stable dielectrics in Mn-modified $(1-x)Bi_{0.5}Na_{0.5}TiO_3$–$xCaTiO_3$ ceramics. *J Electroceram* 2010, **25**: 212–217.

[9] Cao W, Li W, Zhang T, *et al*. High-energy storage density and efficiency of $(1-x)$[0.94NBT–0.06BT]–xST lead-free ceramics. *Energy Technology* 2015, **3**: 1198–1204.

[10] Li WL, Cao WP, Xua D, *et al*. Phase structure and piezoelectric properties of NBT–KBT–BT ceramics prepared by sol–gel flame synthetic approach. *J Alloys Compd* 2014, **613**: 181–186.

[11] Hiruma Y, Imai Y, Watanabe Y, *et al*. Large electrostrain near the phase transition temperature of $(Bi_{0.5}Na_{0.5})TiO_3$–$SrTiO_3$ ferroelectric ceramics. *Appl Phys Lett* 2008, **92**: 262904.

[12] Wang T, Du H, Shi X. Dielectric and ferroelectric properties of $(1-x)Na_{0.5}Bi_{0.5}TiO_3$–$xSrTiO_3$ lead-free piezoceramics system. *J Phys: Conf Ser* 2009, **152**: 012065.

[13] Wang Y, Wang Z, Xu H, *et al*. Properties of $(1-x)Bi_{0.5}Na_{0.5}TiO_3$–$xSrTiO_3$ ferroelectric thin films prepared by metalorganic solution deposition. *J Alloys Compd* 2009, **484**: 230–232.

[14] Hao J, Bai W, Li W, *et al*. Phase transitions, relaxor behavior, and electrical properties in $(1-x)(Bi_{0.5}Na_{0.5})TiO_3$–$x(K_{0.5}Na_{0.5})NbO_3$ lead-free piezoceramics. *J Mater Res* 2012, **27**: 2943–2955.

[15] Shimizu H, Guo H, Reyes-Lillo SE, *et al*. Lead-free antiferroelectric: $x CaZrO_3$–$(1-x)NaNbO_3$ system ($0 \leqslant x \leqslant 0.10$). *Dalton Trans* 2015, **44**: 10763–10772.

[16] Karimi S, Reaney IM, Han Y, *et al.* Crystal chemistry and domain structure of rare-earth doped $BiFeO_3$ ceramics. *J Mater Sci* 2009, **44**: 5102–5112.

[17] Karimi S, Reaney IM, Levin I, *et al*. Nd-doped $BiFeO_3$ ceramics with antipolar order. *Appl Phys Lett* 2009, **94**: 112903.

[18] Li F, Zuo R, Zheng D, *et al*. Phase-composition-dependent piezoelectric and electromechanical strain properties in $(Bi_{1/2}Na_{1/2})TiO_3$–$Ba(Ni_{1/2}Nb_{1/2})O_3$ lead-free ceramics. *J Am Ceram Soc* 2015, **98**: 811–818.

[19] Jo W, Schaab S, Sapper E, *et al*. On the phase identity and its thermal evolution of lead free $(Bi_{1/2}Na_{1/2})TiO_3$–6mol%$BaTiO_3$. *J Appl Phys* 2011, **110**: 074106.

[20] Zhang W, Xue S, Liu S, *et al*. Structure and dielectric properties of $Ba_xSr_{1-x}TiO_3$-based glass ceramics for energy storage. *J Alloys Compd* 2014, **617**: 740–745.

[21] Wang Z, Cao M, Yao Z, *et al*. Dielectric relaxation behavior and energy storage properties in $SrTiO_3$ ceramics with trace amounts of ZrO_2 additives. *Ceram Int* 2014, **40**: 14127–14132.

[22] Wang X, Zhang Y, Song X, *et al*. Glass additive in barium titanate ceramics and its influence on electrical breakdown strength in relation with energy storage properties. *J Eur Ceram* Soc 2012, **32**: 559–567.

[23] Young SE, Zhang JY, Hong W, *et al*. Mechanical self-confinement to enhance energy storage density of antiferroelectric capacitors. *J Appl Phys* 2013, **113**: 054101.